

# ScenePilot-Bench: A Large-Scale Dataset and Benchmark for Evaluation of Vision-Language Models in Autonomous Driving

Yujin Wang<sup>a,1</sup>, Yutong Zheng<sup>a,1</sup>, Wenxian Fan<sup>a</sup>, Tianyi Wang<sup>b</sup>, Hongqing Chu<sup>a</sup>, Dixin Tian<sup>c</sup>, Bingzhao Gao<sup>a,f,\*</sup>, Jianqiang Wang<sup>d</sup>, Hong Chen<sup>e</sup>

<sup>a</sup>*College of Automotive and Energy Engineering, Tongji University, Shanghai, 201804, China*

<sup>b</sup>*Department of Civil, Architectural, and Environmental Engineering, The University of Texas at Austin, Austin, TX, 78712, USA*

<sup>c</sup>*School of Transportation Science and Engineering, Beihang University, Beijing, 100191, China*

<sup>d</sup>*School of Vehicle and Mobility, Tsinghua University, Beijing, 100084, China*

<sup>e</sup>*College of Electronic and Information Engineering, Tongji University, Shanghai, 201804, China*

<sup>f</sup>*State Key Laboratory of Autonomous Intelligent Unmanned Systems, Tongji University, Shanghai, 201210, China*

---

## Abstract

In this paper, we introduce ScenePilot-Bench, a large-scale first-person driving benchmark designed to evaluate vision-language models (VLMs) in autonomous driving scenarios. ScenePilot-Bench is built upon ScenePilot-4K, a diverse dataset comprising 3,847 hours of driving videos, annotated with multi-granularity information including scene descriptions, risk assessments, key participant identification, ego trajectories, and camera parameters. The benchmark features a four-axis evaluation suite that assesses VLM capabilities in scene understanding, spatial perception, motion planning, and GPT-Score, with safety-aware metrics and cross-region generalization settings. We benchmark representative VLMs on ScenePilot-Bench, providing empirical analyses that clarify current performance boundaries and identify gaps for driving-oriented reasoning. ScenePilot-Bench offers a comprehensive framework for evaluating and advancing VLMs in safety-critical autonomous driving contexts.

**Keywords:** Autonomous Driving, Vision-Language Models, Dataset, Benchmark

---

<sup>\*</sup>Corresponding author. Email: gaobz@tongji.edu.cn

<sup>1</sup>These authors contributed equally to this work.

## 1. Introduction

### 1.1. Motivation

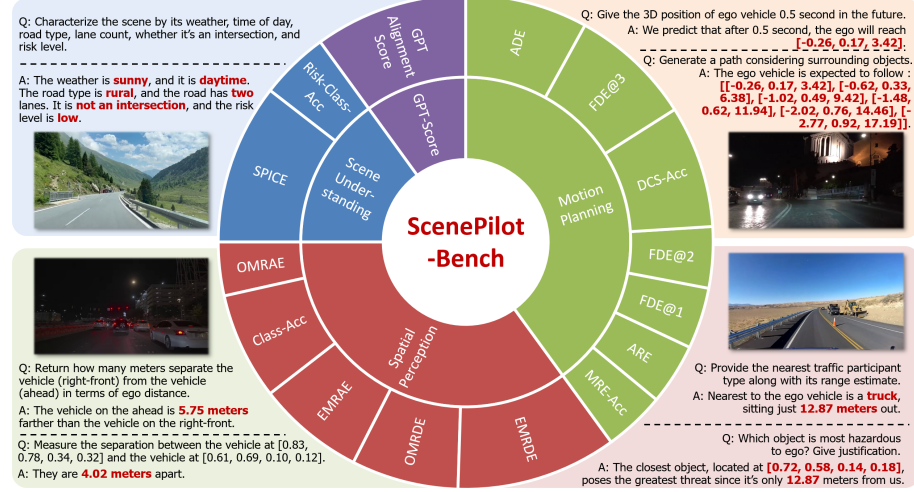


Figure 1: The overall structure of ScenePilot-Bench benchmark. Built upon the ScenePilot-4K dataset, ScenePilot-Bench emphasizes four critical metrics for VLM evaluation in autonomous driving: Scene Understanding, Spatial Perception, Motion Planning, and GPT-Score. Based on large scale data, ScenePilot-Bench could be adopted for both training and evaluation of VLMs and other end-to-end pipelines for autonomous driving.

Vision-Language Models (VLMs) have increasingly been used beyond generic captioning and recognition, and have been integrated into safety-critical autonomy stacks where spatially grounded reasoning and action-aware understanding have become first-order requirements. This trend has naturally aligned autonomous driving with the broader emerging notion of Spatial Embodied Intelligence: an agent’s ability to perceive the environment [1], interpret geometry and interactions in an ego-centric reference frame, and produce decisions that remain valid under real-world physical constraints and implicitly enforced traffic conventions.

Despite rapid progress, reliable evaluation has remained a bottleneck for Spatial Embodied Intelligence in real driving. Existing analyses have repeatedly shown that VLMs may hallucinate ungrounded objects, attributes, and relations, and that such perception-reasoning errors have tended to persist, which has made generic leader-

boards insufficient for diagnosing failures in context [2]. Meanwhile, driving has amplified these issues because the environment is open-world and long-tailed, and errors have directly translated into unsafe or implausible behaviors [3]. Recent driving-oriented VLM efforts have coupled 3D perception, trajectory generation, and language reasoning to improve interpretability, yet evaluation has often been conducted on limited datasets, narrow task slices, or single-domain settings that have not fully stressed geometric consistency, risk-aware planning priors [4], and cross-region robustness[5].

From a system perspective, VLMs have acted more like driving "Co-Pilots" than full end-to-end controllers: they provide scene narratives, identify salient participants, infer risks, and supply decision priors to downstream planning modules, especially in long-tail scenarios where purely learned controllers have shown limited generalization. This role has required an evaluation tool that has jointly measured (i) global semantic understanding and safety reasoning, (ii) ego-centric and object-centric spatial perception, and (iii) motion planning behaviors that have remained physically feasible and risk-aware. Crucially, such an evaluation has also needed to reflect domain shifts that embody cultural and regulatory differences, since traffic rules and driving norms have varied across countries but have rarely been explicit in the visual input.

### 1.2. Contribution

As illustrated in Fig. 1, we present a comprehensive dataset-and-benchmark suite that has served as a practical evaluation instrument for Spatial Embodied Intelligence in autonomous driving. Our contributions are as follows:

- **ScenePilot-4K dataset.** We curate ScenePilot-4K, a large-scale first-person driving video dataset with substantial geographic diversity and long-tail coverage. The dataset is annotated through a unified pipeline that aligns scene descriptions, risk levels, key participants, ego trajectory, and camera parameters on the same clips, enabling consistent evaluation across language grounding, safety reasoning, spatial perception, and motion planning.
- **ScenePilot-Bench benchmark.** Based on ScenePilot-4K, we develop ScenePilot-Bench, an open-loop benchmark that structures VLM capability into four co-

herent modules: scene understanding, spatial perception, motion planning, and GPT-Score. A clip-based protocol has been used to improve temporal stability, and safety-aware metrics and weighting strategies have been designed to connect model outputs to meaningful driving failure modes rather than superficial correctness.

- **Robustness and generalization protocols.** To go beyond in-domain evaluation, we introduce cross-region generalization settings, including Leave-One-Country-Out (LOCO) and right-to-left adaptation, to quantify VLM robustness under distribution shifts that reflect real-world driving variations.
- **Empirical benchmarking and diagnostic analyses.** We benchmark representative commercial and open-source VLMs on ScenePilot-Bench, providing extensive empirical analyses that clarify the current performance boundary of driving-oriented reasoning and identify gaps for future improvement.

## 2. Related Works

### 2.1. Former Representative Specialized Datasets for Autonomous Driving

Training VLMs on dedicated datasets that cover diverse driving scenarios is a key means to improving spatial perception and scene comprehension.

Early works focus on core perception primitives and urban semantics, represented by KITTI [6] and Cityscapes [7], while larger-scale resources such as Waymo Open Dataset [8] and BDD100K [9] extend coverage to complex traffic and multi-task video annotations. Language grounding for driving emerges in Li et al. [10] and Talk2Cars [11], and risk-aware reasoning is further emphasized by DRAMA [12] and DRAMA-ROLISP [13]. For holistic sensing and decision-making, nuScenes [14] provides multi-sensor 360° annotations, while Waymo Open Motion [15], nuPlan [16], Argoverse 2 [17], and Lyft Level-5 [18] shift the focus toward multi-agent prediction and planning with dense trajectories and map context. More recent datasets stress scalability and geographic diversity: OpenDV-2K [19] leverages internet videos with VLM-generated

annotations, Rank2Tell [20] couples dense spatiotemporal attributes with language rationales, and ApolloScape [21] complements with fine-grained semantics and high-precision geo information in complex Chinese urban traffic.

## 2.2. *System Evaluation Based on Standardized Benchmarks*

Constructing evaluation benchmarks that systematically measure how VLMs are deployed in autonomous driving is essential. Existing frameworks have evolved from single-task metrics to multi-dimensional assessments of perception, reasoning, and decision-making, and now mainly follow two paradigms: open-loop and closed-loop.

Open-loop evaluation focuses on intermediate tasks without directly controlling the vehicle. DriveLM [22] introduces a Graph Visual Question Answering (GVQA) task that links perception, prediction, and planning questions in a graph to test multi-modal reasoning. DriveBench [23] evaluates VLM reliability under 17 input conditions and shows that models often over-rely on priors and hallucinate when visual input is corrupted or absent, motivating grounding-sensitive metrics. NuPrompt [24] builds an object-centric prompt set on nuScenes with language descriptions to assess fine-grained perception and language alignment, while STRIDE-QA [25] targets spatiotemporal understanding, interaction reasoning, and causal explanation in driving scenes.

Closed-loop evaluation directly measures how model outputs affect control behavior. BENCH2ADVLM [26] proposes a hierarchical framework that adapts high-level commands into mid-level actions and supports closed-loop testing in simulation or on vehicles, with a self-reflective scenario generator to probe safety-critical failures. In practice, however, VLMs in autonomous driving are typically used as complementary modules to mitigate weak generalization and limited spatial perception rather than to execute full control. As a result, open-loop benchmarks are a practical default to evaluate their overall capability. Based on this insight, we propose ScenePilot-Bench, a new large-scale open-loop benchmark.

### 3. ScenePilot-4K Dataset

#### 3.1. Overview of the Dataset

We present ScenePilot-4K, a large-scale first-person dataset tailored for training and evaluating VLMs in autonomous driving. The dataset not only enables effective learning but also establishes a unified benchmark for comprehensive performance evaluation across diverse and challenging driving conditions. To our knowledge, ScenePilot-4K is among the largest first-person, pure-vision driving video datasets with unified multi-task annotations in the field. It is constructed from high-quality first-person driving videos collected from Bilibili and YouTube. Building upon the publicly available OpenDV-2K dataset [19], which consists of over 1,700 hours of YouTube driving footage, we have augmented it with approximately 2,000 additional hours of driving videos. As a result, our dataset reaches an unprecedented scale of 3,847 hours.

All videos are processed through a high-quality annotation pipeline. Specifically, raw videos are uniformly sliced at a fixed sampling rate, and each segment is annotated using a VLM for scene understanding and risk assessment. Key traffic participants are identified using YOLO11s [27]. Furthermore, we integrate algorithms such as VGGT [28] to estimate both intrinsic and extrinsic camera parameters, as well as to generate accurate trajectory annotations.

##### 3.1.1. Diversity and Advantages over Prior Relevant Datasets

As shown in Table 1, ScenePilot-4K dataset shows great diversity and advantages over prior relevant datasets, namely in the following aspects:

**Scale.** ScenePilot-4K aggregates 3,847 hours of driving videos with 27.7M front-view frames, making it among the largest video corpora for autonomous driving. Although some planning datasets report tens of millions of frames, none of them pair scale with the multi-task, language-grounded supervision offered here.

**Geographic diversity.** As shown in Fig. 2, the dataset spans 63 countries/regions and 1,210 cities, far exceeding the predominantly single-country coverage of most benchmarks (often 1–6 cities). Even compared with the most geographically varied prior work ( $\geq 40$  countries and  $\geq 244$  cities), ScenePilot-4K increases country coverage

Table 1: Comparison among different baseline datasets and our introduced ScenePilot-4K dataset. (a) Scale-related statistics. (b) Annotation availability.

Dataset	Duration	Front-view Frames	Countries & Regions	Cities
KITTI [6]	1.4h	15K	1 (GER)	1
nuScenes [14]	5.5h	214K	2 (USA & SGP)	2
Waymo Open Perception [8]	11h	approx. 390K	1 (USA)	3
Waymo Open Motion [15]	574h	20.7M	1 (USA)	6
BDD100K [9]	approx. 1,000h	318K (MOT)	1 (USA)	2
Cityscapes [7]	0.5h	25K	3 (GER & neighbors)	50
Argoverse 2 [17]	4.2h	300K	1 (USA)	6
ApolloScape [21]	103min	12K	1 (CHN)	1
nuPlan [16]	1282h	62.5M	2 (USA & SGP)	4
ONCE [29]	approx. 144h	approx. 1M	1 (CHN)	Not Released
Lyft Level-5 [18]	approx. 1,000h	approx. 62.5M	1 (USA)	1
Talk2Car [11]	4.7h	9.2K	2 (USA & SGP)	2
OpenDV-2K [19]	2,059h	65.1M	$\geq 40$	$\geq 244$
<b>ScenePilot-4K (ours)</b>	<b>3,847h</b>	<b>27.7M*</b>	<b>63**</b>	<b>1210**</b>

(a) Scale-related statistics.

Dataset	Scene Desc.	Risk Assess.	Key Partic.	Ego Traj.	Cam. Params
KITTI [6]	×	×	✓	✓ (from ego pose)	✓
nuScenes [14]	×	×	✓	✓ (from ego pose)	✓
Waymo Open Perception [8]	×	×	✓	✓ (from ego pose)	✓
Waymo Open Motion [15]	×	×	✓	✓ (from ego pose)	✓
BDD100K [9]	✓ (only labels)	×	✓	✓ (from ego pose)	×
Cityscapes [7]	×	×	✗	✓ (from ego pose)	✓
Argoverse 2 [17]	✓ (meta data)	×	✓	✓ (from ego pose)	✓
ApolloScape [21]	✓ (only labels)	×	✓	✓ (from ego pose)	✓
nuPlan [16]	✓ (only labels)	×	✓	✓ (from ego pose)	✓
ONCE [29]	✓ (only labels)	×	✓	✓ (from ego pose)	✓
Lyft Level-5 [18]	✓ (structured)	×	✓	✓ (from ego pose)	✓
Talk2Car [11]	×	×	✓	✓ (from ego pose)	✓
OpenDV-2K [19]	✓	×	✗	✗	✗
<b>ScenePilot-4K (ours)</b>	✓	✓	✓	✓	✓

(b) Annotation availability.

\*Frame sampling rate 2 Hz. \*\*Obtained based on video filenames.

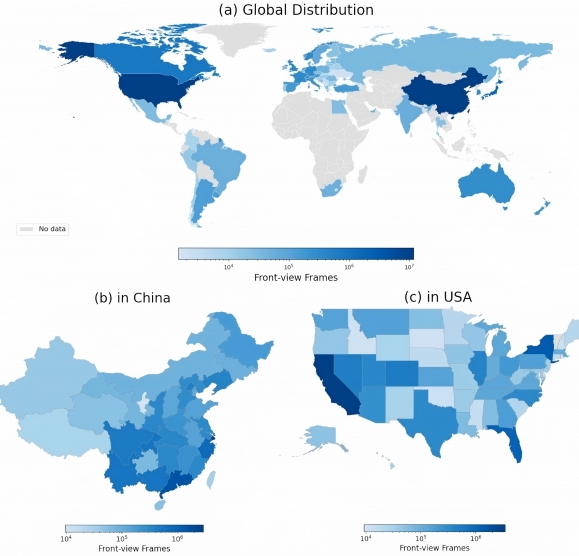


Figure 2: The geographic distribution of ScenePilot-4K dataset. The dataset covers the majority of developed countries as well as countries and regions with relatively well-established infrastructure.

by over 50% and city coverage by about an order of magnitude. This breadth naturally captures diverse road infrastructures, signage systems, traffic behaviors, and driving conventions (e.g., left- vs. right-hand traffic), improving out-of-distribution robustness.

**Annotation richness.** ScenePilot-4K is, to our knowledge, the only dataset that jointly provides all of the following on the same clips: (i) scene-level natural-language descriptions, (ii) risk assessment labels, (iii) key-participant identification, (iv) ego-trajectory, and (v) camera parameters. In contrast, prior datasets typically offer only perception labels (boxes/segments) or metadata-derived ego trajectories, and when language or risk information is available it is usually limited ("only labels/meta-data") and not aligned with trajectory or calibration information. This unified, multi-granularity supervision enables learning objectives that bridge vision-language understanding, risk assessing, agent saliency, and planning-aware prediction within a single benchmark.

### 3.1.2. Detailed Dataset Statistics

As illustrated in Fig. 3, ScenePilot-4K covers diverse real-world conditions, with scenario statistics broadly matching everyday driving (clear-weather dominance and

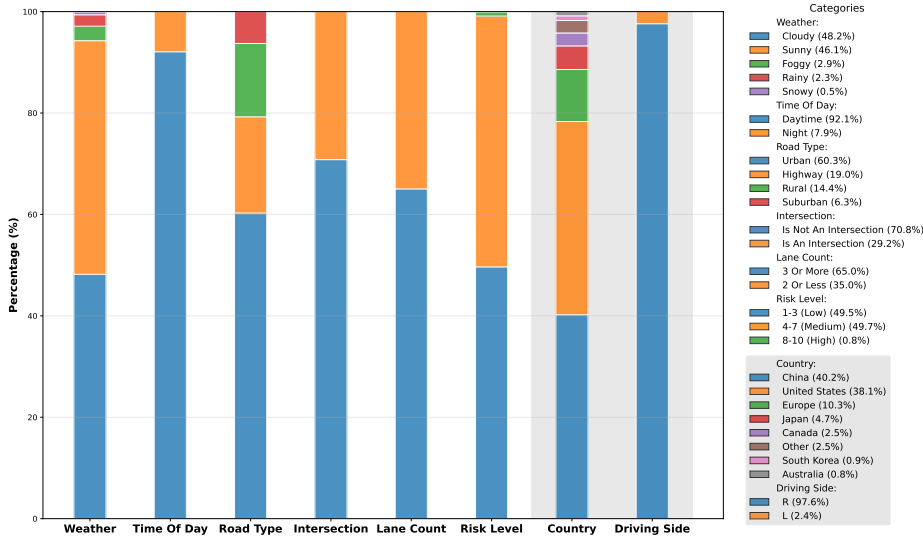


Figure 3: ScenePilot-4K Dataset Statistics: Distribution of Scene Attributes and Driving Countries. This figure summarizes the overall distribution of scene attributes and geographic coverage in the ScenePilot-4K dataset.

limited but non-negligible night-time coverage). The risk distribution is intentionally long-tailed, preserving a small yet essential fraction of high-risk clips to support stress-testing of perception and reasoning. Moreover, the dataset spans multiple countries/regions and includes both right- and left-hand traffic conventions, which facilitates out-of-distribution evaluation under cross-regional shifts.

### 3.2. The High-quality Annotation Pipeline

As shown in Fig. 4, we conduct a high-quality annotation pipeline that produces the multi-task labels required by ScenePilot-Bench. Specifically, the pipeline consists of the following steps:

#### 3.2.1. Video Clipping and Frame Sampling

Raw first-person driving videos are preprocessed by removing the first and last 180 seconds. Within the valid range, frames are uniformly sampled at 2 FPS. The sampled frames are segmented into non-overlapping clips of 5 seconds, corresponding

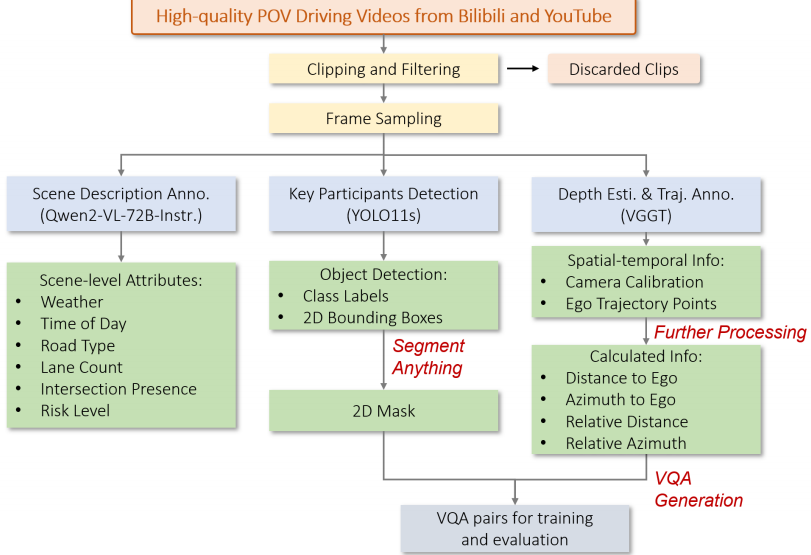


Figure 4: The high-quality annotation pipeline of ScenePilot-4K dataset.

to 10 frames per clip. This pipeline supports large-scale batch processing with resume functionality and consistent data structure.

### 3.2.2. Scene Description and Risk Assessment

We apply a cross-modal annotation module to generate both a semantic scene description and a risk level score for each video clip. This process is automated using Qwen2-VL-72B-Instruct [30] VLM.

For each video clip of  $G = 10$  consecutive frames, only the 4th frame is selected as a representative key frame. The annotated scene description is formatted as: *The weather is sunny, and it is daytime. The road type is urban and the road has four lanes. It is an intersection, and the risk level score is 4.*

### 3.2.3. Key Participant Detection and Annotation

We detect traffic participants using YOLO11s [27] with class-specific confidence thresholds. Given significant variation in object scale and visual distinctiveness, we define a per-class confidence threshold  $\tau_c$  for each category  $c \in C$ , where:

$$C = \{\text{vehicle, truck, bicycle, motorcycle, pedestrian}\} \quad (1)$$

We set  $\tau_{\text{vehicle}} = 0.5$ ,  $\tau_{\text{truck}} = 0.6$ ,  $\tau_{\text{bicycle}} = 0.4$ ,  $\tau_{\text{motorcycle}} = 0.55$ ,  $\tau_{\text{pedestrian}} = 0.55$ , balancing recall and false positives by allowing frequent, reliable classes to use lower thresholds and applying stricter filtering to rarer or more ambiguous ones.

Besides, we store a JSON record per object (ID, label, normalized box), which can be directly combined with camera intrinsics and extrinsics.

### 3.2.4. Camera Calibration and Ego-Trajectory Annotation

We estimate camera intrinsics, extrinsics, and per-frame ego-trajectory using the pre-trained VGGT model [28]. This enables frame-level geometric reasoning and future trajectory labeling without external sensors.

Given the video clip of 10 consecutive frames  $\{I_t\}_{t=1}^{10}$ , we apply VGGT to jointly infer camera parameters. The model outputs per-frame pose encodings, which are converted to camera matrices using calibrated functions.

Extrinsics are converted to camera-to-world matrices  $\mathcal{T}_t^{c2w} \in \mathbb{R}^{4 \times 4}$  via SE(3) inversion. Matrices are adjusted to ensure positive translation values, yielding consistent world coordinate alignment.

We define the ego-trajectory as the camera centers  $\mathbf{C}_t$  across frames, expressed in the first frame’s world coordinate system. Each camera center is computed as:

$$\mathbf{C}_t = (-R_t^\top t_t) - (-R_1^\top t_1), \quad (2)$$

where  $(R_1, t_1)$  are from frame  $t = 1$ . Small positional offsets are applied for stability. The result is a sequence of  $T = 10$  world-frame positions:

$$\mathcal{T}_{\text{ego}} = \{\mathbf{C}_t\}_{t=1}^{10} \in \mathbb{R}^{10 \times 3}. \quad (3)$$

### 3.2.5. Further Processing

After obtaining per-frame camera intrinsics/extrinsics and ego trajectory with VGGT, we perform a lightweight geometric post-processing stage that: (i) lifts 2D evidence to 3D, (ii) recovers metric scale, (iii) extracts foregrounds for key participants, and (iv) reports robust ego-centric distances, azimuths, and inter-agent proximities suitable for VLM/VLA training and evaluation. The pipeline is fully automatic and runs per clip.

**3D lifting from monocular geometry.** For frame  $t$ , pixel  $\mathbf{u} = (u, v)$ , and depth  $\hat{Z}_t(\mathbf{u})$ ,

$$\mathbf{p}_t^c(\mathbf{u}) = \hat{Z}_t(\mathbf{u}) K_t^{-1} \tilde{\mathbf{u}}, \quad \tilde{\mathbf{u}} = [u, v, 1]^\top, \quad (4)$$

where  $\mathbf{p}_t^c(\mathbf{u}) \in \mathbb{R}^3$  is the back-projected 3D point in the camera frame (under VGGT units),  $K_t \in \mathbb{R}^{3 \times 3}$  is the intrinsic matrix, and  $\tilde{\mathbf{u}}$  is the homogeneous pixel.

Optionally, transform to the world frame by

$$\tilde{\mathbf{p}}_t^w(\mathbf{u}) = T_t^{c \rightarrow w} [\mathbf{p}_t^c(\mathbf{u})^\top, 1]^\top, \quad (5)$$

where  $T_t^{c \rightarrow w} \in SE(3)$  is the camera-to-world transform and  $\tilde{\mathbf{p}}_t^w(\mathbf{u}) = [(\mathbf{p}_t^w)^\top, 1]^\top$  is the homogeneous world point.

**Metric scale recovery (frame-level with object-level fallback).** To convert VGGT’s arbitrary scale into metric distances, we first estimate a frame-level ground scale and then optionally fall back to class-specific object priors. We sample a grid  $S$  in the lower half of the image, back-project each sample to a 3D point  $p_{t,k}^c = (x_k, y_k, z_k)$  in the frame, and use robust statistics on the vertical coordinates  $|y_k|$  to select ground inliers:

$$m = \text{median}(|y_k|), \quad (6)$$

$$\text{MAD} = \text{median}(|y_k| - m), \quad (7)$$

$$\mathcal{G} = \{k : |y_k| - m| \leq \kappa \cdot \text{MAD}\}, \quad (8)$$

where  $\kappa > 0$  is a fixed threshold (we use  $\kappa \approx 2.5$ ).

For each target  $i$  in frame  $t$ , we then define a single working metric scale  $s_{t,i}$  by combining the frame-level and object-level estimates in a piecewise form:

$$s_{t,i} = \begin{cases} \frac{H_{\text{cam}}}{\text{median}(|y_k| : k \in \mathcal{G})}, & \text{if the frame-level estimate is reliable,} \\ \frac{H_{c(i)}}{(h_{\text{px}}/f_y)\tilde{z}}, & \text{otherwise,} \end{cases} \quad (9)$$

where  $H_{\text{cam}} > 0$  is the nominal camera height,  $H_{c(i)}$  is the canonical physical height for class  $c(i)$ ,  $h_{\text{px}}$  is the bounding-box height in pixels,  $f_y$  is the vertical focal length, and  $\tilde{z}$  is the median foreground depth (in VGGT units) for object  $i$ . In practice, if  $\mathcal{G}$  is empty or unstable, we approximate the numerator term in the first branch using  $m$

instead of median ( $|y_k| : k \in \mathcal{G}$ ). The resulting  $s_{t,i}$  (meters per VGGT unit) is used to scale all subsequent ego-centric and inter-object distance measurements.

**Foreground extraction for key participants.** Given a detection bbox, we obtain a binary mask  $M_{t,i} \subset \Omega$  via SAM [31], with the bbox as the prompt, and then refine it with light morphology:

$$M_{t,i} = \text{Close}(\text{Open}(\text{SAM}(\text{bbox}, I_t))), \quad (10)$$

where  $I_t \in \mathbb{R}^{H \times W \times 3}$  is the RGB image, and Open/Close are standard  $3 \times 3$  morphological operations. For vehicles, we ignore a thin bottom strip during seeding to reduce road leakage; if SAM inference fails or the bbox is overly large,  $M_{t,i}$  falls back to the rectangle. The set of 3D foreground points is

$$\mathcal{P}_{t,i} = \{\mathbf{p}_t^c(\mathbf{u}) : \mathbf{u} \in M_{t,i}\}. \quad (11)$$

**Robust ego-centric distance and azimuth.** Define per-point radii  $d_j = \|\mathbf{p}_{t,i,j}^c\|_2$  for  $\mathbf{p}_{t,i,j}^c \in \mathcal{P}_{t,i}$ . We report a robust distance using a small percentile:

$$\tilde{d}_{t,i} = \text{perc}_5(\{d_j\}), \quad D_{t,i} = \max\{0, s_{t,i} \tilde{d}_{t,i}\}, \quad (12)$$

where  $\text{perc}_5$  is the 5th percentile operator,  $\tilde{d}_{t,i}$  is in VGGT units, and  $D_{t,i}$  is in meters. For directional context,

$$\bar{\mathbf{p}}_{t,i}^c = \frac{1}{|\mathcal{P}_{t,i}|} \sum_{\mathbf{p} \in \mathcal{P}_{t,i}} \mathbf{p}, \quad \theta_{t,i} = \text{atan2}(\bar{x}, \bar{z}), \quad (13)$$

where  $\bar{\mathbf{p}}_{t,i}^c = (\bar{x}, \bar{y}, \bar{z})$  is the foreground centroid in the camera frame and  $\theta_{t,i} \in \left[-\frac{\pi}{2}, \frac{\pi}{2}\right]$  is the left/right azimuth (radians) relative to the forward axis.

**Inter-agent proximity.** For targets  $i$  and  $j$  in the same frame,

$$\delta_{i \rightarrow j} = \text{perc}_5\left(\left\{\min_{\mathbf{q} \in \mathcal{P}_{t,j}} \|\mathbf{p} - \mathbf{q}\|_2 : \mathbf{p} \in \mathcal{P}_{t,i}\right\}\right), \quad (14)$$

where  $\delta_{i \rightarrow j}$  is a robust, directed separation in VGGT units. The symmetric metric proximity is

$$\Delta_t(i, j) = s_t^* \cdot \min\{\delta_{i \rightarrow j}, \delta_{j \rightarrow i}\}, \quad s_t^* = \frac{1}{2} (s_{t,i} + s_{t,j}), \quad (15)$$

where  $\Delta_t(i, j)$  is in meters and  $s_t^*$  averages the two targets' scales.

**Output.** For each frame, we save for each detection  $i : D_{t,i}, \theta_{t,i}$ , class label, bbox, and a *scale\_info* record indicating whether  $s_t^{\text{frame}}$  or  $s_{t,i}^{\text{obj}}$  was used (with diagnostics such as inlier counts/MAD). We also persist masks and 3D points (VGGT units and metric via  $s_{t,i}$ ) for reproducibility.

#### 4. ScenePilot-Bench Benchmark

To systematically evaluate VLMs’ comprehensive perception and reasoning capability in multi-task driving scenarios, we propose ScenePilot-Bench on top of ScenePilot-4K. Generally, we decompose VLMs’ competence into four modules:

- **Scene Understanding**, which aims to assess VLMs’ global semantic comprehension and risk reasoning ability;
- **Spatial Perception**, which is designed to measure the recognition and classification of key traffic participants, and spatial inference capability of VLMs;
- **Motion Planning**, which evaluates VLMs’ capability to generate future meta-actions and physically feasible trajectories.
- **GPT-Score**, which aims to evaluate the semantic alignment between the answer and the reference using AI tools.

All metrics are computed per clip (10 frames): we aggregate frame-level errors within a clip, convert them to a clip-level score, and average over all clips, which improves temporal stability. This clip-based protocol enhances temporal consistency and mitigates the influence of sporadic noisy frames, leading to a more stable and reliable assessment of model behaviors in real-world driving scenarios.

This section elaborates on the metric design, computational formulation, and conceptual interpretation for each module in detail.

##### 4.1. Scene Understanding

###### 4.1.1. Refined SPICE

SPICE (Semantic Scene Consistency) [32] evaluates the semantic propositional consistency between model-generated and reference scene graphs. We adopt a refined

SPICE with a lightweight, Python-based parser tailored for autonomous driving. It uses a rule-based approach with domain-specific heuristics to extract key traffic participants and attribute tuples, avoiding dependency parsing. Relation tuples are deliberately omitted to reduce noise and improve robustness.

Formally, given a generated scene description  $c$  and a ground truth description  $S$ , they are both parsed into tuple sets  $T(G(c))$  and  $T(G(S))$ . Each tuple includes a unary object tuple ( $o$ ) and an attribute tuple ( $o, a$ ). Precision ( $P$ ), Recall ( $R$ ), and the final SPICE score are defined as:

$$P(c, S) = \frac{|T(G(c)) \otimes T(G(S))|}{|T(G(c))|}, \quad (16)$$

$$R(c, S) = \frac{|T(G(c)) \otimes T(G(S))|}{|T(G(S))|}, \quad (17)$$

$$\text{SPICE}(c, S) = F_1(c, S) = \frac{2 P(c, S) \cdot R(c, S)}{P(c, S) + R(c, S)}, \quad (18)$$

where  $\otimes$  denotes tuple matching with stemming and synonym normalization. A higher SPICE indicates better global semantic consistency.

#### 4.1.2. Risk-Class-Acc: Risk Reasoning Accuracy

We introduce Risk-Class-Acc to quantify VLMs' performance in risk classification tasks:

$$\text{Risk-Class-Acc} = \frac{1}{N} \cdot \sum_{i=1}^N I(r_i^{\text{pred}} = r_i^{\text{gt}}), \quad (19)$$

where  $I(\cdot)$  denotes the indicator function, while  $r_i^{\text{pred}}$  and  $r_i^{\text{gt}}$  represent the predicted and ground-truth risk classes, respectively. The risk classes are divided into three categories: low, medium, and high. This metric reflects VLMs' ability to perform safety-critical reasoning at the semantic level.

## 4.2. Spatial Perception

This section assesses VLMs' spatial perception ability to detect and interpret key traffic participants, such as vehicles, trucks, pedestrians, bicycles and motorcycles, under complex traffic scenarios. It consists of two modules: Object Classification and Spatial Reasoning.

#### 4.2.1. Object Classification

In addition to recognition accuracy, VLMs are also required to possess precise category classification capability. We compute the overall accuracy directly on the entire test set as the core evaluation metric:

$$\text{Class-Acc} = \frac{1}{N} \sum_{i=1}^N I(c_i^{\text{pred}} = c_i^{\text{gt}}), \quad (20)$$

where  $N$  is the total number of samples across all traffic participant categories, namely vehicle, truck, pedestrian, bicycle and motorcycle. This metric comprehensively reflects the overall recognition ability of VLMs across all categories.

#### 4.2.2. Spatial Reasoning

To evaluate spatial reasoning, we measure relative positional and angular errors between the ego vehicle and traffic participants, as well as among participants.

Ego-centric metrics, which include Mean Relative Distance Error to Ego (EMRDE) and Mean Relative Angle Error to Ego (EMRAE), evaluate the relative position of each traffic participant with respect to the ego vehicle:

$$\text{EMRDE} = \frac{1}{N} \sum_{i=1}^N \frac{|\hat{d}_i - d_i|}{d_i}, \quad (21)$$

$$\text{EMRAE} = \frac{1}{N} \sum_{i=1}^N \frac{|\hat{\theta}_i - \theta_i|}{\max(|\theta_i|, \epsilon)}, \quad (22)$$

where  $d_i$  and  $\theta_i$  are the ground truth distance and azimuth between  $i$ th participant and the ego vehicle, while  $\hat{d}_i$  and  $\hat{\theta}_i$  are the predicted values of VLMs, and  $\epsilon$  is a small positive constant for numerical stability.

Object-centric metrics, which include Mean Relative Distance Error inter Object (OMRDE) and Mean Relative Angle Error inter Object (OMRAE), evaluate pairwise relationships among detected objects:

$$\text{OMRDE} = \frac{1}{N} \sum_{i=1}^N \frac{|\hat{d}_{ij} - d_{ij}|}{d_{ij}}, \quad (23)$$

$$\text{OMRAE} = \frac{1}{N} \sum_{i=1}^N \frac{|\hat{\theta}_{ij} - \theta_{ij}|}{\max(|\theta_{ij}|, \epsilon)}, \quad (24)$$

where  $d_{ij}$  and  $\theta_{ij}$  are the ground truth distance and azimuth between  $i$ th and  $j$ th participants, while  $\hat{d}_{ij}$  and  $\hat{\theta}_{ij}$  are the predicted values of VLMs, and  $\epsilon$  is a small positive constant for numerical stability.

These indicators collectively assess spatial coherence and VLMs' ability to infer inter-object geometric dependencies.

#### 4.3. Motion Planning

This module evaluates VLMs' dynamic reasoning ability, including both high-level meta-action prediction and low-level trajectory planning.

##### 4.3.1. Meta-action Prediction

We define meta-actions based on acceleration and heading change trends derived from the annotated ground-truth 3-second future trajectory. Given a trajectory sequence  $(x_t, y_t, z_t)$ , the velocity  $v_t$  and acceleration  $a_t$  are computed as:

$$v_t = \frac{\sqrt{(x_{t+1} - x_t)^2 + (y_{t+1} - y_t)^2 + (z_{t+1} - z_t)^2}}{t_{t+1} - t_t}, \quad (25)$$

$$a_t = \frac{v_{t+1} - v_t}{t_{t+1} - t_t}, \quad (26)$$

and the heading and its change are defined as:

$$\theta_t = \text{atan2}(z_{t+1} - z_t, x_{t+1} - x_t), \quad (27)$$

$$\Delta\theta_t = \theta_{t+1} - \theta_t. \quad (28)$$

We define six meta-actions describing longitudinal and lateral behaviors, as summarized in Table 2.

Table 2: Meta-action Classification Based on Acceleration and Change of Heading

Behavior Type	Acceleration ( $a$ )	Heading Change ( $\Delta\theta$ )
Accelerating	$a \geq +0.15m/s^2$	–
Braking	$a \leq -0.15m/s^2$	–
Constant Speed	otherwise	–
Left Turn	–	$\Delta\theta \geq +8^\circ$
Right Turn	–	$\Delta\theta \leq -8^\circ$
Go Straight	–	otherwise

The Direction-Consistency Accuracy (DCS-Acc) is therefore introduced, which measures whether the VLM-predicted meta-action is consistent with the ground truth. DCS-Acc is formulated as follows:

$$\text{DCS-Acc} = \frac{1}{N} \sum_{i=1}^N I(A_i^{pred} = A_i^{gt}), \quad (29)$$

where  $A_i^{pred}$  denotes meta-actions predicted by VLMs, and  $A_i^{gt}$  denotes the ground truth.

We further use relative and quantitative metrics, such as Mean Relative Acceleration Error (MRE-Acc) and Angular Relative Error (ARE) defined as follows:

$$\text{MRE-Acc} = \frac{1}{N} \sum_{i=1}^N \frac{|a_i^{pred} - a_i^{gt}|}{|a_i^{gt}|}, \quad (30)$$

$$\text{ARE} = \frac{1}{N} \sum_{i=1}^N \frac{|\Delta\theta_i^{pred} - \Delta\theta_i^{gt}|}{\max(|\Delta\theta_i^{gt}|, \epsilon)}. \quad (31)$$

#### 4.3.2. Trajectory Planning

Trajectory planning focuses on spatial accuracy and temporal stability of the VLM-predicted paths [33]. Two standard metrics are employed: Average Displacement Error (ADE) and Final Displacement Error (FDE@T):

$$\text{ADE} = \frac{1}{N} \sum_{i=1}^N \|\hat{p}_i - p_i\|_2, \quad (32)$$

$$\text{FDE@T} = \|\hat{p}_T - p_T\|_2. \quad (33)$$

ADE measures global spatial consistency, while FDE emphasizes endpoint accuracy. We report FDE@1s, FDE@2s, and FDE@3s to assess short-, mid-, and long-term prediction performance.

#### 4.4. GPT-Score

We report GPT-Score, a semantic evaluation metric computed with GPT-4o[34]. For each instance, GPT-4o receives the prompt, ground truth answer, and VLM prediction, and outputs a scalar in  $[0, 1]$  measuring their semantic alignment (higher is better). For full-scene description and risk-reasoning samples, we additionally provide SPICE, Risk-Class-Acc, and the ground-truth risk level as auxiliary inputs. For other question types, GPT-4o only sees the prompt, ground truth, and prediction.

#### 4.5. Evaluation Weighting Strategy

##### 4.5.1. Normalization

All metrics in the benchmark are normalized into a standardized score range of  $[0, 100]$  for non-error-based metrics, and  $(0, 100]$  for error-based metrics. We distinguish non-error-based and error-based metrics, and separate normalization strategies tailored to their mathematical characteristics.

**Non-error-based Metrics:** Non-error-based metrics include SPICE, Risk-Class-Acc, Class-Acc, DCS-Acc, and GPT-Score. These metrics naturally take values in  $[0, 1]$ , and exhibit a simply "higher is better" monotonicity. For these metrics, we adopt a direct linear scaling to obtain a normalized score:

$$S_{non-error} = 100 \times M, \quad (34)$$

where  $M$  denotes the raw metric value.

**Error-based Metrics:** Error-based metrics include EMRDE, EMRAE, OMRDE, OMRAE, MRE-Acc, ARE, ADE, and FDE@T. These metrics quantify deviations between predictions and ground truth, and therefore follow a simply "lower is better" monotonic behavior. We therefore use a piecewise normalization, mapping raw error

Table 3: Normalization Parameters for Error-Based Metrics

Metrics / Parameters	$x_1$	$x_2$	$k$
EMRDE	0.1135	0.3856	9.1380
EMRAE	0.1052	0.4055	2.2210
OMRDE	0.1244	0.4252	8.0125
OMRAE	0.1155	0.4152	2.0542
MRE-Acc	0.7250	1.3056	0.0216
ARE	0.7588	1.3319	0.0125
ADE	2.2850	5.2278	7.2514
FDE@1	1.3595	3.7750	6.7157
FDE@2	1.3595	3.7750	6.7157
FDE@3	1.3595	3.7750	6.7157

$E$  to  $(0, 100]$ , which could be defined as:

$$S_{\text{error}}(E; x_1, x_2, k) = \begin{cases} 100, & E < x_1, \\ 100 - 40 \frac{E - x_1}{x_2 - x_1}, & x_1 \leq E < x_2, \\ 60 \exp(-k(E - x_2)), & E \geq x_2, \end{cases} \quad (35)$$

where  $x_1$  is the high precision threshold,  $x_2$  is the acceptable error threshold, and  $k > 0$  is an exponential decay factor.

We first estimate the normalization parameters for each error-based metric using the empirical error distributions from a representative set of baseline models. These parameters are then fixed and applied consistently to all subsequent model evaluations. Specifically, we set the high-precision threshold  $x_1$  to the 15th percentile, and the acceptable error threshold  $x_2$  to the 75th percentile of the raw errors. Thus, only the top 15% most accurate predictions receive a perfect score of 100, and the worst 25% predictions are mapped to the exponential penalty region.

This formulation provides the following desirable properties:

- **High-precision region ( $E < x_1$ ):** Errors below a high-precision threshold are rewarded uniformly with a perfect score of 100, reflecting negligible deviation in practice.

- **Moderate-error region ( $x_1 \leq E < x_2$ ):** Scores decrease linearly from 100 to 60, enabling fine-grained comparison among VLMs with moderate errors.
- **High-error region ( $E \geq x_2$ ):** Scores decay exponentially from 60 to 0, maintaining continuity while strongly penalizing large, potentially unsafe or physically infeasible errors more than small ones, in line with safety-critical evaluation in autonomous driving.

Table 3 lists the normalization parameters for all error-based metrics, showing how each maps into the unified scoring space.

#### 4.5.2. The Overall Weighting Strategy

Table 4: Weighting structure of the evaluation framework of ScenePilot-Bench benchmark

Module	Module Weight	Metric	Metric Weight
Scene Understanding	0.15	SPICE	0.70
		Risk-Class-Acc	0.30
Spatial Perception	0.35	Class-Acc	0.20
		EMRDE	0.30
		EMRAE	0.20
		OMRDE	0.20
		OMRAE	0.10
Motion Planning	0.40	DCS-Acc	0.20
		MRE-Acc	0.10
		ARE	0.10
		FDE@1	0.10
		FDE@2	0.10
		FDE@3	0.20
		ADE	0.20
GPT-Score	0.10	GPT Alignment Score	1.00

As shown in Table 4, the evaluation framework adopts a structured weighting strategy that reflects the functional roles and safety relevance of different system capabilities.

Within each module, individual metrics are further weighted based on their operational significance. Within scene understanding, we prioritize semantic robustness measured by SPICE, while still allocating substantial weight to risk classification due to its safety relevance. Spatial Perception emphasizes ego-relative distance and angle

errors, which directly affect collision risk, while inter-object metrics capture interaction reasoning complexity. Motion Planning integrates both dynamic correctness and multi-horizon endpoint accuracy (FDE@1/2/3), reflecting the increasing difficulty and importance of long-term trajectory prediction, complemented by ADE for overall trajectory consistency.

#### 4.6. *Geographic Generalization*

To comprehensively evaluate VLMs’ robustness and adaptability across unseen geographic regions and camera calibrations, we design a systematic generalization assessment protocol comprising two cross-domain settings. No new metrics are introduced in this section.

**LOCO (Leave-One-Country-Out) Evaluation.** We adopt a LOCO strategy to assess geographic robustness. For each target country, VLMs are trained on data from all other countries and evaluated exclusively on the held-out country’s test set.

**Right-to-Left Adaptation.** Driving environment differs significantly between left-hand and right-hand traffic systems. To evaluate VLMs’ adaptability to this fundamental shift, we introduce a cross-traffic evaluation:

- R→L: Train exclusively on right-hand traffic countries (e.g., China, US), test on left-hand traffic countries (e.g., Japan, UK).

Performance drop relative to an in-domain baseline measures resilience to new traffic rules, which means that smaller drop reflects better generalization.

#### 4.7. *Discussion*

The proposed benchmark establishes a comprehensive evaluation pipeline encompassing scene understanding, spatial perception, and motion planning. It systematically connects high-level reasoning with low-level geometric consistency, forming an overall assessment of multi-modal driving intelligence. By jointly considering objective spatial precision, subjective semantic plausibility, and further geographic generalization, our benchmark enables a holistic understanding of model performance in real-world driving contexts.

## 5. Experiments

### 5.1. Comparative Experiments of Various VLMs on ScenePilot-Bench Benchmark

In the Comparative experiment of various VLMs on ScenePilot-Bench benchmark, the original dataset is partitioned into training, validation, and test sets respectively. The training set is used for VLM fine-tuning, the validation set for hyperparameter tuning and model selection, and the test set for final performance evaluation. The split follows a principle of multidimensional conditional uniformity, jointly accounting for weather conditions, road types, lane configurations, intersection attributes, risk levels, traffic density, and geographic regions to ensure balanced representation across all subsets.

In constructing the VQA dataset, samples for the training and test sets are independently drawn from their respective video splits to rigorously prevent data leakage. Each VQA sample is associated with a unique video clip, ensuring no overlap between training and test samples. This design guarantees that model evaluation reflects true generalization to unseen scenarios. Although we annotate nearly 400 million VQA samples for the entire dataset, such a volume is unnecessary for the current fine-tuning of VLMs. In the comparative experiment, the training and test sets contain 200,000 and 100,000 VQA samples, respectively, which are sufficient to demonstrate the effectiveness of our proposed method. The full annotated dataset could be used in the future to train the foundational capabilities of VLMs.

In this work, we fine-tune VLMs using Parameter-Efficient Fine-Tuning (PEFT) strategies within the Unsloth optimization framework. Experiments were conducted on four NVIDIA A800 GPUs employing a Distributed Data Parallel (DDP) strategy. To balance memory efficiency with numerical stability, we utilized Bfloat16 precision throughout the process, in conjunction with the 8-bit AdamW optimizer.

Table 5 and Fig. 5 function as a structured comparison across three model regimes: (i) commercial and large open-source VLMs without driving-specific fine-tuning, (ii) the ReasonDrive-7B model and its fine-tuned variants, and (iii) our proposed ScenePilot models obtained by fine-tuning the corresponding Qwen backbones on the ScenePilot-4K dataset. This partition clarifies where performance gains come from and which

Table 5: Comparison of various VLMs on ScenePilot-Bench benchmark.

(a) Scene Understanding and Spatial Perception.

Model	Scene Understanding			Spatial Perception					
	SPICE	Risk-Class-Acc	total	Class-Acc	EMRDE	EMRAE	OMRDE	OMRAE	total
GPT-4o[34]	92.93	74.82	87.50	91.93	49.57	22.51	26.23	22.23	45.23
GPT-5[35]	92.18	71.64	86.01	91.83	57.58	25.83	19.37	23.92	47.07
Qwen2.5-VL-72B[36]	92.87	73.54	87.07	91.71	46.39	14.58	13.06	21.64	39.95
Gemini-2.5-flash[37]	91.70	69.44	85.02	92.55	54.39	22.70	22.24	24.63	46.28
Qwen3-VL-235B[38]	93.58	77.23	88.68	91.64	57.92	14.99	21.87	21.61	45.24
ReasonDrive-7B[39]	85.31	33.84	69.86	75.12	74.10	7.27	10.00	52.22	45.92
ReasonDrive-7B-trained	85.45	37.06	70.93	89.27	71.81	26.83	31.44	71.28	58.18
ReasonDrive-7B-CoT[39]	85.51	34.07	70.08	88.55	53.88	7.36	8.51	36.87	40.73
ReasonDrive-7B-CoT-trained	87.90	56.91	78.60	90.18	68.81	22.16	23.93	51.51	53.05
ScenePilot-2-2B-200k	93.64	80.57	89.72	85.74	87.76	73.67	48.41	50.75	72.97
ScenePilot-2.5-3B-200k	<b>93.65</b>	78.67	89.15	86.19	<b>87.98</b>	<b>73.69</b>	<b>52.58</b>	<u>55.78</u>	<b>74.46</b>

(b) Motion Planning, GPT-Score and Overall Score.

Model	Motion Planning							GPT-Score	Overall
	DCS-Acc	MRE-Acc	ARE	ADE	FDE@1	FDE@2	FDE@3		
GPT-4o[34]	15.79	82.16	85.07	58.68	85.79	42.71	24.15	49.30	22.56
GPT-5[35]	22.39	81.32	79.59	57.53	85.25	44.88	28.20	50.73	36.51
Qwen2.5-VL-72B[36]	15.78	80.43	85.02	34.58	62.46	25.85	9.80	37.41	30.15
Gemini-2.5-flash[37]	19.59	76.73	79.89	43.77	76.40	34.10	19.63	43.31	33.64
Qwen3-VL-235B[38]	22.80	43.83	83.05	12.69	15.70	8.67	5.55	23.33	34.22
ReasonDrive-7B[39]	14.38	29.45	61.23	13.67	23.31	11.25	9.09	19.95	15.70
ReasonDrive-7B-trained	10.50	<b>95.25</b>	<b>93.01</b>	<b>98.26</b>	<b>99.51</b>	<b>97.48</b>	<b>82.95</b>	<b>76.87</b>	27.60
ReasonDrive-7B-CoT[39]	14.12	0.49	47.55	0.00	0.00	0.00	0.00	7.63	17.90
ReasonDrive-7B-CoT-trained	11.14	<b>99.55</b>	<b>95.18</b>	<b>98.21</b>	<b>99.54</b>	<b>97.52</b>	<b>82.70</b>	<b>77.59</b>	24.72
ScenePilot-2-2B-200k	<u>28.46</u>	79.47	75.07	59.31	82.72	47.78	29.16	51.89	<u>52.53</u>
ScenePilot-2.5-3B-200k	<b>29.52</b>	88.20	70.09	53.07	79.94	43.64	32.67	51.24	<b>54.43</b>
									<b>65.01</b>

capabilities remain bottlenecks under driving-oriented evaluation.

For commercial and large open-source VLMs, the results show strong scene-level semantics. These models typically produce fluent and plausible descriptions, reflected in high SPICE scores, and Fig. 5 reflects this advantage in the scene-understanding axis. However, their relative strength weakens once the benchmark shifts from semantic plausibility to embodied correctness, especially in Spatial Perception and Motion Planning. This gap indicates that generic multi-modal pretraining transfers well to high-level understanding and coarse semantics, but it does not reliably induce the ego-centric calibration and reference-frame consistency required for precise spatial reason-

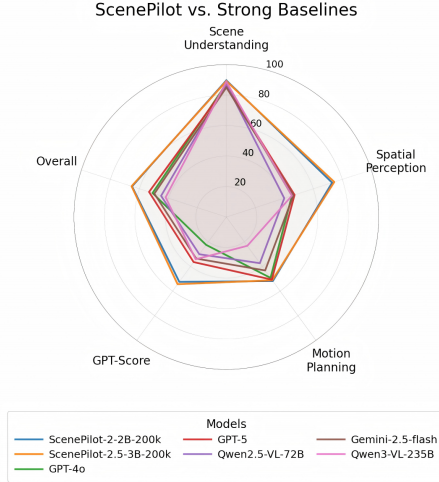


Figure 5: An intuitive performance comparison between the Qwen-series models fine-tuned on the ScenePilot-4K dataset and baseline models (both commercial and large-scale open-source VLMs).

ing, relation grounding, nor the rule-sensitive dynamics needed for motion planning.

As a driving-specialized VLM, ReasonDrive-7B [39] exhibits a task-oriented bias that differs from general-purpose models. The trained results, where we fine-tune ReasonDrive-7B on the ScenePilot-4K dataset, show significant improvements across all modules compared to the original model. This demonstrates the effectiveness of our dataset in enhancing driving-specific capabilities. Especially, as a VLM mostly for motion planning, ReasonDrive-7B-trained and ReasonDrive-7B-CoT-trained VLMs achieve leading performance in motion planning metrics, as shown in Table 5b.

The most salient shift appears for our ScenePilot models, which we obtain by directly fine-tuning the corresponding Qwen backbones. Compared with both general-purpose large models and ReasonDrive-7B variants, ScenePilot models present a more balanced and robust competence profile: they preserve strong scene semantics while expanding Spatial Perception and Motion Planning more substantially, which Fig. 5 clearly illustrates. This behavior indicates that ScenePilot supervision strengthens not only language expression but also the coupling between visual grounding, spatial reasoning, and dynamic prediction. Notably, ScenePilot-2.5-3B-200k attains the highest overall score of 65.37, outperforming all other models. This result highlights the ef-

ficiency of our dataset and training approach in eliciting driving-relevant capabilities even from moderate-sized backbones.

Overall, the three-block organization of Table 5 and Fig. 5 supports a practical conclusion: (i) general-purpose VLMs provide strong semantic baselines but remain limited in embodied grounding; (ii) a driving-specialized model benefits from fine-tuning yet does not automatically achieve holistic robustness; (iii) directly fine-tuning a capable backbone on a well-constructed driving dataset like ScenePilot-4K yields the most balanced and effective driving VLMs. This insight guides future development toward integrated datasets and training strategies that jointly cultivate semantics, perception, and planning.

### *5.2. The Experiment on Geographic Generalization of VLMs*

In the country-generalization experiment, China is selected as the training domain with 200,000 VQA samples. The test set is divided into four subsets based on geographic regions: Europe (EU), Japan and South Korea (JP/KR), the United States (US), and other countries (OTH). Each subset contains 100,000 VQA samples drawn from their respective video splits. This design allows for a rigorous evaluation of VLMs’ ability to generalize to unseen geographic domains with distinct traffic rules, road structures, and cultural contexts. In the generalization experiment on the right-to-left adaptation, we train VLMs exclusively on right-hand traffic countries with 200,000 samples. We then form a candidate test set from left-hand traffic countries, and sample 100,000 instances.

Table 6 reports the geographic generalization results when the Qwen2.5-VL-3B model is trained exclusively on China and evaluated on four unseen regions, together with a right-to-left traffic adaptation setting. The results indicate that the model maintains a remarkably stable overall performance across unseen regions, with Overall Scores ranging from 67.17 to 70.32, reflecting strong geographic generalization. This narrow spread suggests that a substantial portion of the learned capability transfers effectively across diverse traffic systems and road structures.

A finer-grained breakdown reveals a consistent hierarchy in cross-domain robustness. Scene-level semantic understanding transfers best, as SPICE stays essentially

Table 6: The Experiment on Geographic Generalization of VLMs.

(a) Scene Understanding and Spatial Perception.

Model	Scene Understanding			Spatial Perception					
	SPICE	Risk-Class-Acc	total	Class-Acc	EMRDE	EMRAE	OMRDE	OMRAE	total
SP-2.5-3B-CN (EU)	92.57	75.26	87.37	83.44	91.53	67.33	54.37	54.38	73.92
SP-2.5-3B-CN (JP/KR)	92.48	71.01	86.04	83.84	89.36	68.50	53.91	56.60	73.72
SP-2.5-3B-CN (US)	92.74	74.75	87.34	83.18	90.33	69.04	56.72	56.76	74.56
SP-2.5-3B-CN (OTH)	91.99	70.14	85.44	83.09	92.35	71.16	57.74	56.68	75.77
SP-2.5-3B-R (L)	93.72	78.79	89.24	90.51	85.21	74.17	54.51	57.10	75.11

(b) Motion Planning, GPT-Score and Overall Score.

Model	Motion Planning								GPT-Score	Overall
	DCS-Acc	MRE-Acc	ARE	ADE	FDE@1	FDE@2	FDE@3	total		
SP-2.5-3B-CN (EU)	12.72	65.11	50.20	75.33	74.40	69.76	70.24	57.60	54.54	67.47
SP-2.5-3B-CN (JP/KR)	12.80	68.83	53.03	75.37	70.61	67.03	69.18	57.42	54.96	67.17
SP-2.5-3B-CN (US)	11.69	64.03	51.27	81.18	72.53	69.79	76.78	59.69	54.14	68.49
SP-2.5-3B-CN (OTH)	12.73	66.95	52.17	84.67	81.50	78.11	80.30	63.41	56.22	70.32
SP-2.5-3B-R (L)	10.95	54.68	47.68	78.95	80.77	74.95	73.70	58.53	54.61	68.55

saturated across all regions. In contrast, risk assessment is more sensitive, which is expected because risk perception is shaped by local traffic rules, road user behaviors, and infrastructures that vary across countries. Spatial perception remains broadly functional under domain shifts. Across all regions, the overall Spatial Perception score is consistently maintained at approximately 74, while Class-Acc is highly stable around 83. However, the separation largely stems from the combined behavior of geometric metrics (EMRDE, EMRAE, OMRDE, OMRAE), which are more sensitive to visual domain shifts that affect depth cues and spatial relationships. This pattern suggests that the regional gap is unlikely to be explained by country or language alone, rather, it is more plausibly driven by visual-geometric statistics that vary with local infrastructure, camera setups, and environmental conditions.

The motion planning module is the most sensitive to domain shift, and the high-level actions are more fragile than trajectory errors. DCS-Acc drops significantly across all regions, indicating that the model struggles to infer correct driving maneuvers under unfamiliar traffic conventions and road layouts. This is expected, as action prediction relies heavily on understanding local driving norms, which vary widely across

countries. In contrast, while trajectory errors also degrade, the impact is less severe. This suggests that while the model’s high-level decision-making falters under domain shifts, its low-level path generation retains some robustness, likely due to learned physical constraints and vehicle dynamics that are more universal.

The left-hand-traffic adaptation results further highlight the challenges of cross-traffic generalization. When trained solely on right-hand traffic countries, the model’s overall performance on left-hand traffic test sets remains stable, but with noticeable degradation compared to in-domain baselines. Scene understanding and spatial perception are relatively preserved, indicating that global scene semantics and object localization are less affected by traffic directionality. However, motion planning suffers more pronounced declines, particularly in DCS-Acc, reflecting the difficulty of adapting high-level driving decisions to fundamentally different traffic rules. This underscores the importance of incorporating diverse traffic scenarios during training to build truly robust autonomous driving models.

## 6. Conclusions

In this paper, we present ScenePilot-4K and ScenePilot-Bench, a dataset-and-benchmark suite for evaluating Spatial Embodied Intelligence in first-person driving scenarios. ScenePilot-4K provides large-scale, geographically diverse driving clips with unified multi-task annotations. Built upon this dataset, ScenePilot-Bench introduces a four-axis evaluation protocol covering Scene Understanding, Spatial Perception, Motion Planning, and GPT-Score, which links language outputs to driving-relevant spatial-temporal factors under a stable clip-based scoring design.

The comparative experiments show a consistent pattern across model regimes. General-purpose commercial and open-source VLMs remain strong in scene-level semantics, but they fall short when evaluation emphasizes ego-centric spatial grounding and decision-consistent planning. Domain-specialized models benefit from fine-tuning, yet they do not automatically yield balanced competence across all modules. In contrast, directly fine-tuning capable backbones on the ScenePilot-4K dataset produces the most integrated and effective driving VLMs, demonstrating the value of our dataset and bench-

mark in cultivating Spatial Embodied Intelligence. The generalization experiments further reveal that while scene semantics and spatial perception transfer robustly across geographic domains, motion planning remains sensitive to local traffic conventions and road structures. This highlights the need for diverse training data to achieve truly adaptable autonomous driving models.

Future work naturally follows three directions: strengthening rule- and culture-aware reasoning to enhance geographic generalization, expanding evaluation toward more challenging long-tail and high-risk interactions with tighter physical constraints, and connecting open-loop VLM evaluation with closed-loop driving simulation to assess end-to-end driving performance.

### Acknowledgment

The dataset and codes will be made publicly available at:

- <https://github.com/yjwangtj/ScenePilot-Bench>;
- <https://huggingface.co/datasets/larswangtj/ScenePilot-4K>.

This research was supported by National Key R&D Program of China (2023YFB2504400), the National Nature Science Foundation of China (No. 62088101, No. 62373289, No. 62273256 and No. 62473291), Shanghai Municipal Science and Shanghai Automotive Industry Science and Technology Development Foundation (No.2407), and the Fundamental Research Funds for the Central Universities.

### References

- [1] X. Hu, Z. Duan, P. An, Y. Zhang, Z. Xu, J. Ma, Dual-domain homogeneous fusion with cross-modal mamba and progressive decoder for 3d object detection, *Pattern Recognition* 172 (2026) 112725.
- [2] T. Huang, Z. Liu, R. Wang, Y. Zhang, L. Jing, Visual hallucination detection in large vision-language models via evidential conflict, *International Journal of Approximate Reasoning* (2025) 109507.

- [3] J. Li, L. Yang, Y. Chen, Y. Jin, Mfan: Mixing feature attention network for trajectory prediction, *Pattern Recognition* 146 (2024) 109997.
- [4] G. Zou, Z. Zhou, R. Weibel, Y. Li, T. Wang, Z. Liu, W. Ding, C. Fu, Multi-graph spatio-temporal network for traffic accident risk forecasting, *Pattern Recognition* (2025) 112784.
- [5] X. Zhou, X. Han, F. Yang, Y. Ma, A. C. Knoll, Opendrivevla: Towards end-to-end autonomous driving with large vision language action model, *arXiv preprint arXiv:2503.23463* (2025).
- [6] A. Geiger, P. Lenz, C. Stiller, R. Urtasun, Vision meets robotics: The kitti dataset, *The international journal of robotics research* 32 (11) (2013) 1231–1237.
- [7] M. Cordts, M. Omran, S. Ramos, T. Rehfeld, M. Enzweiler, R. Benenson, U. Franke, S. Roth, B. Schiele, The cityscapes dataset for semantic urban scene understanding, in: *Proceedings of the IEEE conference on computer vision and pattern recognition*, 2016, pp. 3213–3223.
- [8] P. Sun, H. Kretzschmar, X. Dotiwalla, A. Chouard, V. Patnaik, P. Tsui, J. Guo, Y. Zhou, Y. Chai, B. Caine, et al., Scalability in perception for autonomous driving: Waymo open dataset, in: *Proceedings of the IEEE/CVF conference on computer vision and pattern recognition*, 2020, pp. 2446–2454.
- [9] F. Yu, H. Chen, X. Wang, W. Xian, Y. Chen, F. Liu, V. Madhavan, T. Darrell, Bdd100k: A diverse driving dataset for heterogeneous multitask learning, in: *Proceedings of the IEEE/CVF conference on computer vision and pattern recognition*, 2020, pp. 2636–2645.
- [10] W. Li, Z. Qu, H. Song, P. Wang, B. Xue, The traffic scene understanding and prediction based on image captioning, *IEEE Access* 9 (2020) 1420–1427.
- [11] T. Deruyttere, D. Grujicic, M. B. Blaschko, M.-F. Moens, Talk2car: Predicting physical trajectories for natural language commands, *Ieee Access* 10 (2022) 123809–123834.

- [12] S. Malla, C. Choi, I. Dwivedi, J. H. Choi, J. Li, Drama: Joint risk localization and captioning in driving, in: Proceedings of the IEEE/CVF winter conference on applications of computer vision, 2023, pp. 1043–1052.
- [13] X. Ding, J. Han, H. Xu, W. Zhang, X. Li, Hilm-d: Enhancing mllms with multi-scale high-resolution details for autonomous driving, International Journal of Computer Vision (2025) 1–17.
- [14] H. Caesar, V. Bankiti, A. H. Lang, S. Vora, V. E. Liong, Q. Xu, A. Krishnan, Y. Pan, G. Baldan, O. Beijbom, Nuscenes: A multimodal dataset for autonomous driving, in: Proceedings of the IEEE/CVF Conference on Computer Vision and Pattern Recognition, 2020, pp. 11621–11631.
- [15] S. Ettinger, S. Cheng, B. Caine, C. Liu, H. Zhao, S. Pradhan, Y. Chai, B. Sapp, C. R. Qi, Y. Zhou, et al., Large scale interactive motion forecasting for autonomous driving: The waymo open motion dataset, in: Proceedings of the IEEE/CVF international conference on computer vision, 2021, pp. 9710–9719.
- [16] H. Caesar, J. Kabzan, K. S. Tan, W. K. Fong, E. Wolff, A. Lang, L. Fletcher, O. Beijbom, S. Omari, nuplan: A closed-loop ml-based planning benchmark for autonomous vehicles, arXiv preprint arXiv:2106.11810 (2021).
- [17] B. Wilson, W. Qi, T. Agarwal, J. Lambert, J. Singh, S. Khandelwal, B. Pan, R. Kumar, A. Hartnett, J. K. Pontes, et al., Argoverse 2: Next generation datasets for self-driving perception and forecasting, arXiv preprint arXiv:2301.00493 (2023).
- [18] J. Houston, G. Zuidhof, L. Bergamini, Y. Ye, L. Chen, A. Jain, S. Omari, V. Iglovikov, P. Ondruska, One thousand and one hours: Self-driving motion prediction dataset, in: Conference on Robot Learning, PMLR, 2021, pp. 409–418.
- [19] J. Yang, S. Gao, Y. Qiu, L. Chen, T. Li, B. Dai, K. Chitta, P. Wu, J. Zeng, P. Luo, et al., Generalized predictive model for autonomous driving, in: Proceedings of the IEEE/CVF Conference on Computer Vision and Pattern Recognition, 2024, pp. 14662–14672.

[20] E. Sachdeva, N. Agarwal, S. Chundi, S. Roelofs, J. Li, M. Kochenderfer, C. Choi, B. Dariush, Rank2tell: A multimodal driving dataset for joint importance ranking and reasoning, in: Proceedings of the IEEE/CVF winter conference on applications of computer vision, 2024, pp. 7513–7522.

[21] P. Wang, X. Huang, X. Cheng, D. Zhou, Q. Geng, R. Yang, The apolloscape open dataset for autonomous driving and its application, *IEEE transactions on pattern analysis and machine intelligence* 1 (2019).

[22] C. Sima, K. Renz, K. Chitta, L. Chen, H. Zhang, C. Xie, J. Beißwenger, P. Luo, A. Geiger, H. Li, Drivelm: Driving with graph visual question answering, in: Proceedings of the European Conference on Computer Vision, Springer, 2024, pp. 256–274.

[23] S. Xie, L. Kong, Y. Dong, C. Sima, W. Zhang, Q. A. Chen, Z. Liu, L. Pan, Are vlms ready for autonomous driving? an empirical study from the reliability, data, and metric perspectives, *arXiv preprint arXiv:2501.04003* (2025).

[24] D. Wu, W. Han, Y. Liu, T. Wang, C.-z. Xu, X. Zhang, J. Shen, Language prompt for autonomous driving, in: Proceedings of the AAAI Conference on Artificial Intelligence, Vol. 39, 2025, pp. 8359–8367.

[25] K. Ishihara, K. Sasaki, T. Takahashi, D. Shiono, Y. Yamaguchi, Stride-qa: Visual question answering dataset for spatiotemporal reasoning in urban driving scenes, *arXiv preprint arXiv:2508.10427* (2025).

[26] T. Zhang, T. Jin, L. Wang, J. Liu, S. Liang, M. Zhang, A. Liu, X. Liu, Bench2advlm: A closed-loop benchmark for vision-language models in autonomous driving, *arXiv preprint arXiv:2508.02028* (2025).

[27] G. Jocher, J. Qiu, Ultralytics yolo11 (2024).  
URL <https://github.com/ultralytics/ultralytics>

[28] J. Wang, M. Chen, N. Karaev, A. Vedaldi, C. Rupprecht, D. Novotny, Vggt: Visual geometry grounded transformer, in: Proceedings of the Computer Vision and Pattern Recognition Conference, 2025, pp. 5294–5306.

- [29] J. Mao, M. Niu, C. Jiang, H. Liang, J. Chen, X. Liang, Y. Li, C. Ye, W. Zhang, Z. Li, et al., One million scenes for autonomous driving: Once dataset, arXiv preprint arXiv:2106.11037 (2021).
- [30] P. Wang, S. Bai, S. Tan, S. Wang, Z. Fan, J. Bai, K. Chen, X. Liu, J. Wang, W. Ge, et al., Qwen2-vl: Enhancing vision-language model's perception of the world at any resolution, arXiv preprint arXiv:2409.12191 (2024).
- [31] A. Kirillov, E. Mintun, N. Ravi, H. Mao, C. Rolland, L. Gustafson, T. Xiao, S. Whitehead, A. C. Berg, W.-Y. Lo, et al., Segment anything, in: Proceedings of the IEEE/CVF international conference on computer vision, 2023, pp. 4015–4026.
- [32] P. Anderson, B. Fernando, M. Johnson, S. Gould, Spice: Semantic propositional image caption evaluation, in: European conference on computer vision, Springer, 2016, pp. 382–398.
- [33] C. Li, L. Gong, L. Xu, X. Wang, Difftrajectory: Mitigating cumulative errors and enhancing inference efficiency in diffusion-based trajectory prediction, Pattern Recognition (2025) 112339.
- [34] A. Hurst, A. Lerer, A. P. Goucher, A. Perelman, A. Ramesh, A. Clark, A. Ostrow, A. Welihinda, A. Hayes, A. Radford, et al., Gpt-4o system card, arXiv preprint arXiv:2410.21276 (2024).
- [35] S. Bubeck, C. Coester, R. Eldan, T. Gowers, Y. T. Lee, A. Lupsasca, M. Sawhney, R. Scherrer, M. Sellke, B. K. Spears, et al., Early science acceleration experiments with gpt-5, arXiv preprint arXiv:2511.16072 (2025).
- [36] S. Bai, K. Chen, X. Liu, J. Wang, W. Ge, S. Song, K. Dang, P. Wang, S. Wang, J. Tang, et al., Qwen2. 5-vl technical report, arXiv preprint arXiv:2502.13923 (2025).
- [37] G. Comanici, E. Bieber, M. Schaekermann, I. Pasupat, N. Sachdeva, I. Dhillon, M. Blistein, O. Ram, D. Zhang, E. Rosen, et al., Gemini 2.5: Pushing the fron-

tier with advanced reasoning, multimodality, long context, and next generation agentic capabilities, arXiv preprint arXiv:2507.06261 (2025).

- [38] S. Bai, Y. Cai, R. Chen, K. Chen, X. Chen, Z. Cheng, L. Deng, W. Ding, C. Gao, C. Ge, W. Ge, Z. Guo, Q. Huang, J. Huang, F. Huang, B. Hui, S. Jiang, Z. Li, M. Li, M. Li, K. Li, Z. Lin, J. Lin, X. Liu, J. Liu, C. Liu, Y. Liu, D. Liu, S. Liu, D. Lu, R. Luo, C. Lv, R. Men, L. Meng, X. Ren, X. Ren, S. Song, Y. Sun, J. Tang, J. Tu, J. Wan, P. Wang, P. Wang, Q. Wang, Y. Wang, T. Xie, Y. Xu, H. Xu, J. Xu, Z. Yang, M. Yang, J. Yang, A. Yang, B. Yu, F. Zhang, H. Zhang, X. Zhang, B. Zheng, H. Zhong, J. Zhou, F. Zhou, J. Zhou, Y. Zhu, K. Zhu, Qwen3-vl technical report, arXiv preprint arXiv:2511.21631 (2025).
- [39] A. Chahe, L. Zhou, Reasondrive: Efficient visual question answering for autonomous vehicles with reasoning-enhanced small vision-language models, in: Proceedings of the Computer Vision and Pattern Recognition Conference, 2025, pp. 3870–3879.

#### **Declaration of interest**

The authors declare that they have no known competing financial interests or personal relationships that could have appeared to influence the work reported in this paper.